2025 IEEE International Conference on Robotics and Automation (ICRA)
May 19-23, 2025. Atlanta, USA

Ambient Flow Perception of Freely Swimming Robotic Fish Using an Artificial Lateral Line System

Hongru Dai†, Xiaozhu Lin†, *Graduate Student Member, IEEE*, Kaitian Chao, and Yang Wang, *Member, IEEE*

***Abstract*— Robotic fish hold significant promise as efficient underwater systems, yet their inability to accurately perceive ambient flow hinders their deployment in real-world scenarios. Inspired by the natural lateral line system(LLS), a flow-responsive organ in fish that plays a crucial role in behaviors such as rheotaxis, this paper introduces the first Artificial Lateral Line System (ALLS)-based ambient flow classifier for robotic fish that allows robotic fish to perceive flow fields while swimming freely. To be specific, using just 5 pressure sensors and 3.5 minutes of swimming data, we trained a Long Short-Term Memory (LSTM) network, achieving a classification accuracy of 81.25% across 8 flow speed categories, ranging from 0.08 m/s to 0.18 m/s. A key innovation of this work is the formulation of ambient flow perception as a classification task, which not only enables the robotic fish to extract meaningful information but also enhances the robustness and generalizability of the perception framework. Extensive experiments further identify critical factors such as affecting the effectiveness of the ambient flow classifier, offering valuable insights for future development.**

I. Introduction

Robotic fish have emerged as highly efficient and versatile underwater systems, largely due to their bio-mimetic designs, which have garnered substantial research interest [1]. Extensive research has examined various aspects of robotic fish, including their morphology [2], propulsion mechanisms [3], and control strategies [4]. Despite these advancements, environmental perception—particularly the perception of flow fields—remains a significant challenge for robotic fish, especially in real-world scenarios. In natural aquatic environments such as lakes and rivers, non-stationary ambient flows introduce significant complexities to the inherent fluidic interactions between robotic fish and their surrounding fluids. This affects both the performance of the robotic fish and the accuracy of their flow field perception. Consequently, achieving effective flow field perception for freely swimming robotic fish continues to be a critical and ongoing challenge.

Among conventional hydrodynamic sensing techniques [5]–[7], Artificial Lateral Line System (ALLS) [8] has been gaining attention for its cost-effectiveness and ability to detect subtle changes in water pressure, thereby perceiving the surrounding flow field. Like robotic fish, ALLS [9], [10] is inspired by the natural LLS found in fish, a highly efficient fluid sensing mechanism. One of the earliest applications of ALLS was demonstrated in [11] in which the velocity distribution of Kármán vortices generated by a cylinder is studied and visualized. However, many subsequent researchers [12]–[15] has predominantly focused on employing ALLS for estimating the state of robotic fish—such as velocity [13], [16], [17], posture [6], [18], and trajectory [1]—rather than for ambient flow sensing. However, it has been identified by biologists [19] that the LLS plays a crucial role in various flow-related behaviors in fish, such as rheotaxis (orienting into an oncoming current), obstacle avoidance, and prey localization in a non-stationary flow field. These capabilities demonstrate that fish can not only sense but also perceive the characteristics of the ambient flow field. Therefore, this work focuses on leveraging ALLS for ambient flow perception.

Related research dates back to 2013 when Kruusmaa *et al.* [20] demonstrated that a robotic fish equipped with five pressure sensors could estimate flow speed and identify flow regimes. Subsequent work [21] by Fuentes *et al.* involved upgrading the sensor mechanism and increasing the number of sensors, which led to improved prediction accuracy. Despite the advancements in their ALLS, these robotic fish were constrained to a fixed position, simplifying experimental complexity but failing to account for the effects of the robotic fish's movement on ALLS performance. Liu *et al.* [15], [22] later addressed this limitation by proposing an enhanced carrier model supported by Computational Fluid Dynamics (CFD) and equipped with an ALLS composed of 23 pressure sensors. While this approach improved the accuracy of flow characteristic estimation, the ALLS-equipped carrier did not mimic the shape of a robotic fish nor utilize Body and/or Caudal Fin (BCF) propulsion. Consequently, the influence of vortices generated by the carrier's own motion on the ALLS, which introduces significant noise into the pressure data collected by the ALLS, was not considered. Thus, the findings from these studies [15], [20]–[22] cannot be directly applied to robotic fish that need to perceive ambient flow while swimming freely.

Addressing the clear limitations in existing research [15], [20]–[22] on the flow perception of freely swimming robotic fish using ALLS, this study introduces a straightforward and effective data-driven technique for classifying incoming flow velocities, thereby facilitating the perception of the ambient fluid field. The approach of framing flow perception as a classification problem rather than a precise velocity measurement arises from the fact that: similar to natural fish, the ability of a robotic fish to navigate varying environmental flow speeds is influenced by its size and swimming capabilities.

†Hongru Dai and Xiaozhu Lin are co-first authors and contributed equally to this work. *(Corresponding author: Yang Wang.)*

Hongru Dai, Xiaozhu Lin and Yang Wang are with the School of Information Science and Technology, ShanghaiTech University, Shanghai, China. *(E-mail: {daihr2024, linxzh, wangyang4}@shanghaitech.edu.cn)*

Kaitian Chao is with the School of Information Science and Technology, ShanghaiTech University, Shanghai, China, and with the GRASP Laboratory, University of Pennsylvania, Philadelphia, PA 19104, USA. *(E-mail:chaokt@seas.upenn.edu)*

2025 IEEE International Conference on Robotics and Automation (ICRA) | 979-8-3315-4139-2/25/$31.00 ©2025 IEEE | DOI: 10.1109/ICRA55743.2025.11128034

Authorized licensed use limited to: ShanghaiTech University. Downloaded on March 10,2026 at 06:36:40 UTC from IEEE Xplore. Restrictions apply.

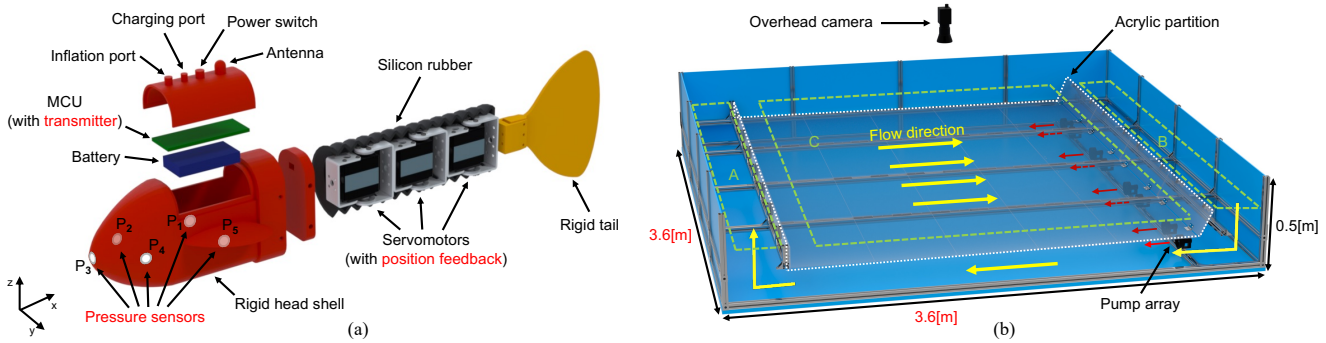

Fig. 1. **Overview of the experimental platform.** (a) There are five pressure sensors: one (P_3) at the tip of the head, two (P_2, P_4) at the middle part of the streamlined section and two (P_1, P_5) at the middle part of the flat part, embedded on the surface of the head. Schematic of interior details of the robotic fish and the entire hardware platform; (b) A customizable swimming pool designed to generate ambient flow fields. Constructed with stainless steel profiles and acrylic sheets, the pool features an acrylic partition separating upper and lower chambers. Submerged pump arrays create left-to-right flow in the upper chamber.

Therefore, the relative magnitude of the ambient flow is often more relevant than the exact speed. By classifying flow velocities, the proposed method provides actionable insights into ambient flow conditions without necessitating precise velocity measurements, making it more adaptable to robotic fish of varying sizes and operational environments.

As a data-driven approach, a key aspect of this work is the efficient acquisition of effective ALLS data. We developed a robotic fish equipped with high-resolution pressure sensors and constructed a pool environment capable of generating a fluid field with a uniform distribution of flow speeds, ranging from high to low. The data-collection procedure initiated by calibrating the static pressure in a still water pool. Subsequently, the pump array was activated to create a carefully designed flow field. We then selected a random trajectory covering various flow speed regions and collected pressure variations recorded by the ALLS while the robotic fish was controlled to follow the targeted path. With the collected data, we evaluated various methods for training the classifier, finding that a Long Short-Term Memory (LSTM) network [23] performed particularly well and the choice of features for online classification significantly impacts algorithm effectiveness. Ultimately, our method achieved a classification accuracy of 81.25% in categorizing incoming flow speed intervals of 0.0125 m/s (with 8 classes for the ambient flow field ranging from 0.08 m/s to 0.18 m/s). Compared to existing works [15], [21], [22], the contribution and innovation of this paper include:

1) This is the first ALLS-based ambient flow classifier that allows robotic fish to distinguish the incoming flow velocity while swimming freely, using a relatively limited amount of data (5 sensors and 3.5 minute of swimming data).
2) Reformulating the ambient flow perception problem as a classification task not only enables the robotic fish to obtain meaningful information but also enhances the robustness and generalizability of the overall framework.
3) This study identifies key factors affecting the effectiveness of the flow velocity classifier, providing valuable insights for future development.

The remainder of this paper is organized as follows. The platform setup is in Section II. Detail procedure of data collection, processing and training is given in Section III. Section IV describes the experiment results and analysis. Finally, conclusions are drawn in Section V.

II. Experimental Platform

In this section, we provide a detailed introduction to the experimental platform of our work, as shown in Fig. 1. The platform includes a robotic fish prototype with ALLS and a swimming pool that can generate a large-scale ambient flow field. In this work, we use this platform to collect the pressure values of the ALLS installed at the head of the robotic fish.

A. Robotic Fish with ALLS

The developed robotic fish mimics a typical carangiform fish with BCF propulsion mode, as depicted in Fig. 1(a). Its dimensions are $0.52\,\mathrm{m} \times 0.13\,\mathrm{m} \times 0.12\,\mathrm{m}$, weighing $1.1\,\mathrm{kg}$. The robotic fish is comprised of three main components: (i) a rigid head housing an MCU board with the ESP32-S3-WROOM-1U module, an $800\,\mathrm{mAh}$ $7.4\,\mathrm{V}$ lithium battery for power and an ALLS composed of pressure sensors array; (ii) a deformable body consisting of three joints connected by aluminum components and covered with rubber skin; and (iii) a rigid tail. The head and tail are 3D-printed from ABS plastic and coated with epoxy resin for waterproofing. Each joint is driven by a Hiwonder LX-824 servomotor with real-time position feedback. Moreover, the pressure sensor in ALLS is TE Connectivity MS5803-01BA, which has a width of $6.2\,\mathrm{mm}$ and a length of $6.4\,\mathrm{mm}$ with the maximum resolution of $1.2\,\mathrm{Pa}$ and $1\,\mathrm{kPa}$ to $130\,\mathrm{kPa}$ scale range, and connected to MCU through IIC bus.

In this work, we focus on the planar motion of the robotic fish, so we adjust the density of the robotic fish to be slightly lower than that of water to make sure that the robotic fish only moves on the planar surface of the water.

B. Ambient Flow Pool

In order to collect various data on the free swimming of robotic fish in different ambient flow fields, we designed and developed a pool that can generate large-scale ambient flow,

Authorized licensed use limited to: ShanghaiTech University. Downloaded on March 10,2026 at 06:36:40 UTC from IEEE Xplore. Restrictions apply.

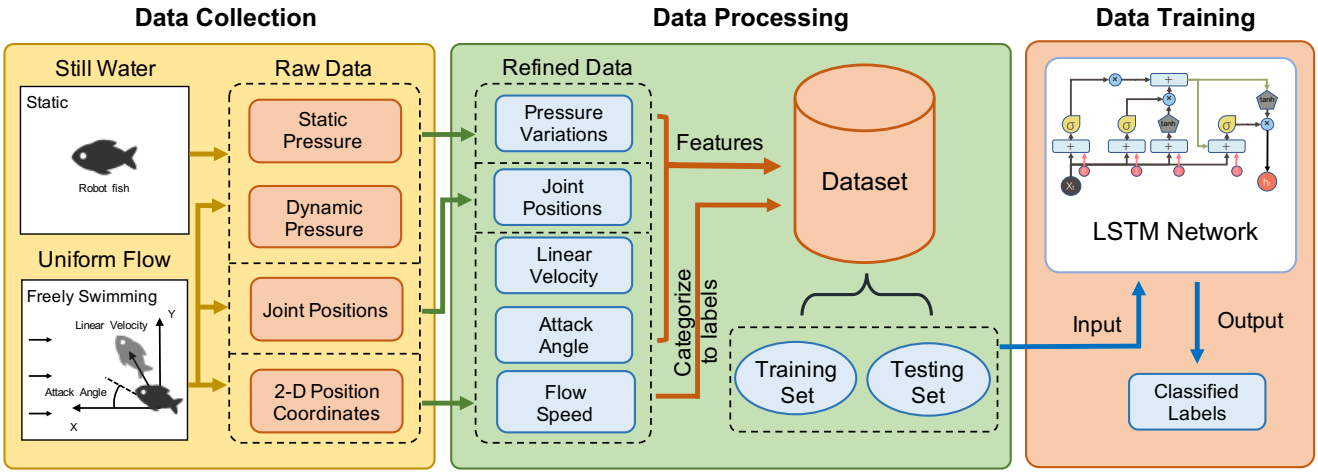

Fig. 2. **Schemitic of the method for learning the proposed ambient flow velocity classifier for a freely swimming robotic fish.** (a) The static pressure was collected in still water and the dynamic pressure and two-dimensional coordinates of the fish's head and body were recorded when the robotic fish was freely swimming. (b) Pressure variations, linear velocity, and attack angle were calculated from raw data as features, while joint positions remained unprocessed. Flow speed was categorized into labels. (c) The dataset included the training set and test set, which was the input of the LSTM network, as the output was the classified labels.

as shown in Fig. 1(b). The swimming pool with dimensions (length $\times$ width $\times$ height) of $3.6\,\mathrm{m} \times 3.6\,\mathrm{m} \times 0.5\,\mathrm{m}$, mainly constructed by stainless steel profiles and acrylic sheets. The water depth is set to $0.4\,\mathrm{m}$ during the experiment. Especially, the pool is divided into upper and lower parts by an acrylic partition. Under the partition, pump array is fixed on stainless steel profiles to push the water to move from right to left, further promoting the ambient flow field of the upper water. In order to clearly depict the velocity field of the ambient flow field, the vane-wheel type flow meter is used to measure the flow speed at a specified location in the flow field.

C. Upper Computer System

In order to control the free swimming of the robotic fish in the pool, the upper computer wirelessly sends control commands to the robotic fish through UDP protocol, and then controls the joints of the robotic fish to swing. In addition, an RGB camera fixed 3 meters above the pool capturing a top-down image of the whole pool, which is used to recognize the position of the robotic fish's head and body and process information such as its linear velocity and attack angle. At the same time, the pressure sensor data collected from the ALLS at the head of the robotic fish and the position feedback of joints will also be wirelessly sent to the upper computer via UDP for subsequent processing. During the experiment, all operations are performed at a frequency of $50\,\mathrm{Hz}$.

III. Methodology

In this section, we provide a detailed description of our method for obtaining an efficient ambient flow speed classifier for a freely swimming robotic fish. As illustrated in Fig. 2, the process consists of three major steps: data collection, data processing, and the design and training of an LSTM neural network. The overall framework is straightforward and efficient. Throughout this description, we will highlight the key factors that influence the effectiveness of the framework, offering insights for practitioners in the related community.

A. Data Collection

As described in Fig. 2(a), the first step involves collecting validate pressure data of ALLS and position data of the robotic fish during the freely swimming. This began with calibrating static pressure in a still water pool by recording sensor readings for over $10\,\mathrm{s}$ with the fish fully submerged. The average of these readings was used as static pressure, with recursive averaging preferred. To counteract environmental effects like temperature, an embedded compensation algorithm was used. Accurate static pressure measurement was crucial for algorithm performance. For the two-dimensional motion of the robotic fish, a single average static pressure sufficed, as tests showed variations within 2 cm depth had minimal impact. For three-dimensional motion, static pressure would need to be recorded at different depths.

Next, dynamic pressure data was collected from the freely swimming robotic fish in a flow pool designed for a uniform current (see Section II B). The flow ranged from $0.08\,\mathrm{m/s}$ to $0.18\,\mathrm{m/s}$ and stabilized 1 minute after activating the pump array, as shown in Fig. 3. True flow velocities were measured using a vane-wheel-type flow meter in the dense grid, with a maximum vertical flow velocity standard deviation of $0.004\,\mathrm{m/s}$, confirming vertical uniformity. To establish the training and testing set configuration described in Section III B, two independent free-swimming trials were conducted under identical flow field conditions. During each 3.5-minute trial, the robotic fish swam freely swam freely along a different trajectory, collecting approximately 10,000 data points at $50\,\mathrm{Hz}$. To cover all flow velocities and movement patterns, 10 target points were randomly selected across the pool in each trial. The fish, controlled by a CPG-PID strategy [24], moved from point to point. Experimental results showed

Authorized licensed use limited to: ShanghaiTech University. Downloaded on March 10,2026 at 06:36:40 UTC from IEEE Xplore. Restrictions apply.

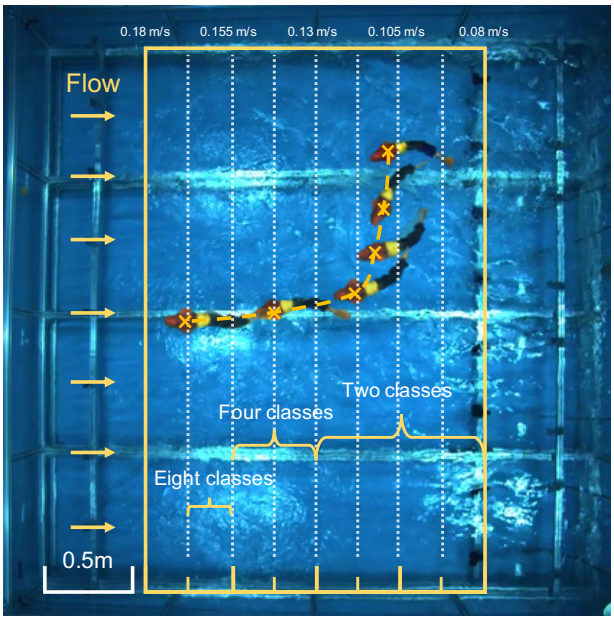

Fig. 3. The distribution and classification of the flow field. The flow velocity above the figure shows the uniformly decreasing flow distribution in the flow pool. The flow field was classified by two, four and eight according to the flow velocity.

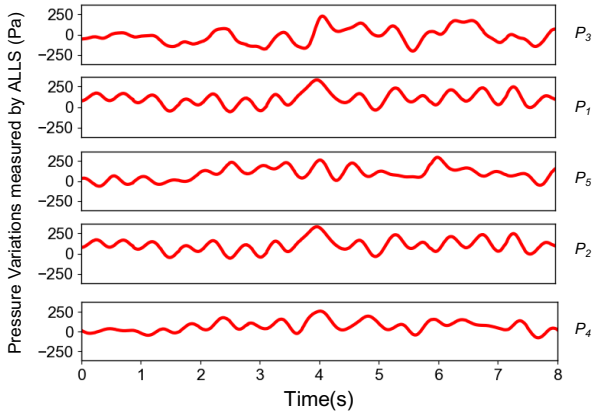

Fig. 4. Real-time pressure variations measured by ALLS when robotic fish was freely swimming.

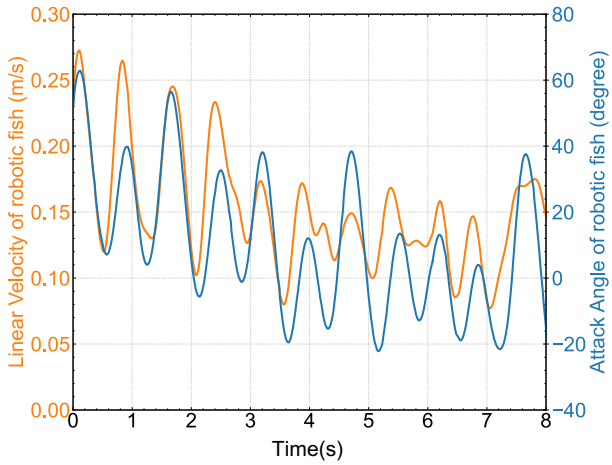

Fig. 5. Real-time linear velocity and attack angle of robotic fish.

that this controller's choice had minimal impact on data quality, provided it ensured small tracking errors and low time costs. The fish's head and body coordinates recorded by an overhead camera and three joint positions were collected for later data processing and classifier training.

B. Data Processing

In this subsection, we outline the procedure for processing raw data to create a dataset for training the flow classification model. First, we obtained dynamic pressure variations by subtracting static pressure from measured dynamic pressure. The attack angle of the robotic fish was calculated from the fish's head orientation relative to the flow, and linear velocity was computed by differentiating the fish head's position over time. Notably, the positions of the three joints were retained without any additional processing. An eight-second data segment, shown in Fig. 4 and Fig. 5, illustrates how pressure variations, linear velocity, and attack angle vary with time. These figures reveal strong periodicity in both the fish's state and pressure data due to the fish's oscillatory movements of the fish's head and tail. This periodic behavior explains why ALLS systems used in fixed setups [20], [21] or non-fish-shaped vehicles [15], [22] cannot be directly applied to freely swimming robotic fish.

Next, the processed features created ten input features for the dataset, as shown in Fig. 3. Each time step's feature vector, using the fish head's position and flow field distribution, was labeled with a flow speed category. We experimented with two class, four class, and eight class categorizations. To structure the data for classification, a sliding window of length T extracted sequences of length T as input features, with the flow speed class at the $T+1$-th time step as the output label. This resulted in a dataset with dimensions $N \times T \times 10$, where N is the total number of samples from the sliding window. The first free-swimming trial was used as the training set, while the second trial was used as the testing set, ensuring that the model was evaluated on entirely unseen data.

C. Data Training

Finally, we developed and trained a LSTM neural network for flow speed classification, chosen for its ability to capture temporal dependencies in time-series data from pressure sensors. Inspired by the biological LLS in fish, which helps them sense changes in surrounding flow fields, we hypothesized that an effective ALLS-based NN classifier should retain historical data, enabling it to capture both short- and long-term dependencies. This approach is expected to enhance the model's generalization and robustness in real-world applications.

The input to the LSTM model included preprocessed pressure data, supplemented with selected motion parameters like the fish's linear velocity, attack angle and three joint positions. Combining pressure data with motion information enabled the network to better grasp the relationship between the fish's movements and the surrounding flow field, leading to improved classification performance. As demonstrated in

Authorized licensed use limited to: ShanghaiTech University. Downloaded on March 10,2026 at 06:36:40 UTC from IEEE Xplore. Restrictions apply.

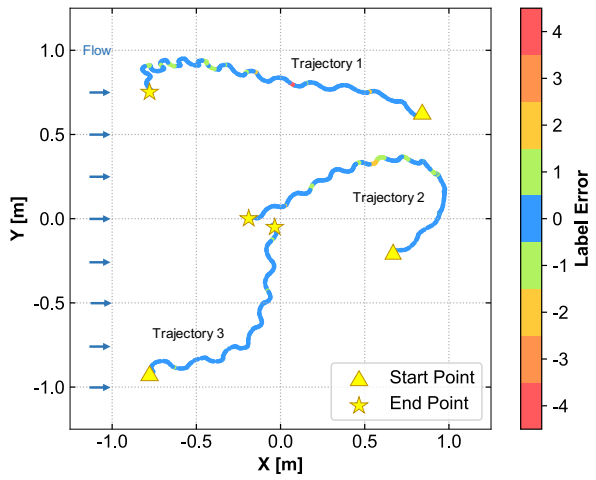

Fig. 6. Results of the eight class classification. Most points are marked in blue, indicating correct classifications. A small number of points, however, are marked in other colors, signifying misclassifications.

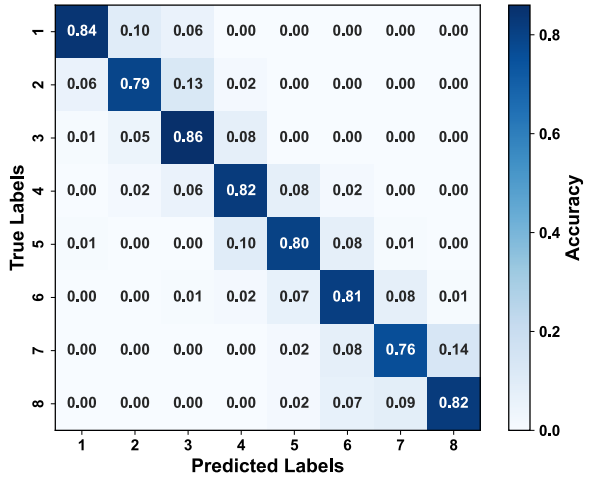

Fig. 7. Confusion matrix of the eight class classification results. The majority of categories show an accuracy rate exceeding 80%.

our experimental results (detailed in the next section), while the LSTM architecture is relatively simple, incorporating relevant motion parameters significantly boosts accuracy. This highlights the crucial role of feature selection in building a model that can effectively classify flow velocities in dynamic, noisy environments.

The architecture and settings of the LSTM model are described in the following subsection. The LSTM network has four layers: an input layer with 128 neurons for time-series features, two hidden layers with 64 and 32 neurons respectively, and an output layer with n neurons, where n is the number of classification labels. The output layer uses a sigmoid activation function in two class tasks, while a softmax activation function is used in multi-class tasks. The model was trained with backpropagation through time (BPTT) and optimized using the Adam optimizer. Performance and design details will be covered in the next section.

To evaluate the LSTM network's performance, we compared it with Random Forest (RF) and Multi-Layer Perceptron (MLP) models. Both RF and MLP were trained and tested using the same dataset as the LSTM, with their structures adjusted accordingly. The RF model employed 200 trees, with parameters optimized via grid search. The MLP model had a structure of $128 \times 64 \times 32 \times n$. ReLU was used for the first three layers, while the final layer used softmax.

TABLE I
THE COMPARISON RESULTS OF SEVERAL ALGORITHMS

Algorithm	T	Two classes	Four classes	Eight classes
LSTM	**250**	**96.69%**	**91.47%**	**81.25%**
	150	94.54%	81.79%	73.09%
	50	87.83%	78.62%	67.84%
RF	**250**	**81.0%**	**61.0%**	**51.3%**
	150	72.19%	58.3%	47.9%
	50	65.0%	49.18%	41.2%
MLP	**250**	**73.18%**	**55.46%**	**37.86%**
	150	72.19%	55.29%	33.0%
	50	70.43%	49.18%	31.62%

IV. EXPERIMENTAL RESULTS AND DISCUSSIONS

In this section, we primarily focus on presenting and analyzing the experimental results. Specifically, we first demonstrate the performance of the LSTM method in classifying flow velocity with high resolution. Following this, other popular machine learning classification algorithms, namely MLP and RF, were also employed for experimentation and compared against the LSTM network. Additionally, we discuss the impact of different time windows on classification accuracy, as well as various classification metrics. Finally, we analyze the impact of different features by training the models with various feature combinations.

A. Classification Performance of LSTM

After training, the LSTM network exhibited strong classification performance, achieving accuracies of 96.69%, 91.47%, and 81.25% for two class, four class, and eight class classifications, respectively. We present the results for the eight class classification as an example. Fig. 6 shows the LSTM network's classification of three robotic fish trajectories from the test set. These three trajectories exhibit diverse behaviors, representing the robotic fish swimming against the flow, crossing the flow with its back to it, and executing turning maneuvers. Additionally, they span all flow speed intervals, demonstrating the diversity of the test set. To visualize the LSTM network's classification performance, each data point in the trajectory is colored based on the difference between its true and predicted labels. Most points are blue, indicating correct classification, while a few consecutive points are green, showing misclassifications into adjacent labels. Fig. 7 provides a detailed view of classification performance through a confusion matrix, with values normalized to reflect accuracy. Most labels were correctly classified, with accuracies over 80%. Overall, the LSTM network demonstrated strong performance in the

Authorized licensed use limited to: ShanghaiTech University. Downloaded on March 10,2026 at 06:36:40 UTC from IEEE Xplore. Restrictions apply.

TABLE II
THE COMPARISON RESULTS OF DIFFERENT FEATURES COMBINATION USING LSTM

Class	All Features	No Velocity	No Angle	No Pressure Variations	No Swimming Data	No $P_{1,5}$	No $P_{2,4}$	No P_3
Two	96.69%	79.25%	58.7%	51.5%	56.7%	84.1%	90.6%	76.3%
Four	91.47%	83.12%	40.12%	26.1%	36.5%	79.5%	85.79%	74.3%
Eight	81.25%	65.03%	26.01%	13.08%	21.3%	62.32%	74.09%	55.13%

classification task. It effectively used pressure data from the ALLS and the robotic fish's swimming behavior to classify ambient flow speed.

B. Comparison of Different Algorithms and Parameters

MLP and RF were also used for comparison in the same classification tasks, with the impact of different time windows on accuracy discussed in Table I. At $T = 250$, where the LSTM used 5 second of prior data, it achieved 96.69%, 91.47%, and 81.25% accuracy in three tasks, respectively. RF reached 81.0%, 61.0%, and 51.3%, while MLP achieved 73.18%, 55.46%, and 37.86%.At $T = 150$, LSTM's accuracy was 94.54%, 81.79%, and 73.09%, while RF achieved 72.19%, 58.3%, and 47.9%. At $T = 50$, LSTM's accuracy dropped to 87.83%, 78.62%, and 67.84%, and RF scored 65.0%, 49.18%, and 41.2%. These findings indicate LSTM consistently outperformed MLP and RF across all time windows, and its accuracy declined more gradually as the window shortened, showing greater robustness.

Fig. 8 shows metrics for the LSTM network with a time window of $T = 250$, including Precision, Recall, and F1 Score, whose mathematical formulations can be found in [25]. In two class classification, these metrics were around 95%, reflecting high accuracy and effective positive sample capture. For four class and eight class tasks, metrics slightly decreased but still showed strong performance. This demonstrates LSTM network's robust generalization and a balanced trade-off between Precision and Recall.

C. Estimation Accuracy of Different Feature Combinations

After evaluating the impact of different classification algorithms and parameters, it's crucial to assess how dataset composition influences performance. We analyzed how various feature combinations affect accuracy using the top-performing LSTM classifier ($T = 250$). Our aim was to identify the most impactful features by training models on datasets with different combinations. The results, shown in Table II, include eight feature sets: the full set, excluding linear velocity, excluding attack angle, only pressure variations, only swimming data (linear velocity, attack angle and three joint positions), and excluding specific pressure sensors.

In two class classification, excluding the robotic fish's velocity caused a moderate accuracy drop, while excluding the attack angle, using only pressure variations, or relying solely on swimming data led to accuracy declines of over 40%. Notably, removing pairs of pressure sensors had minimal impact. Among these, excluding P_3 reduced accuracy more than excluding $P_{1,5}$ or $P_{2,4}$. Similar trends were observed

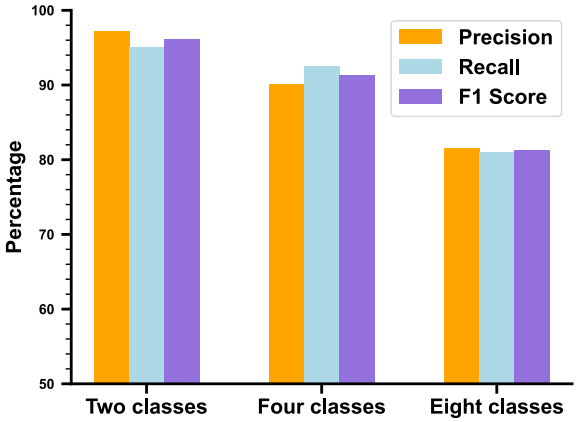

Fig. 8. This bar chart presents the classification metrics of the LSTM network across different classification tasks, including Precision, Recall, and F1 score, which are critical indicators for evaluating classifier performance. All metrics achieve high performance across multiple classification tasks.

in more granular classifications. As classification granularity increased, the absence of linear velocity had a more significant effect, showing its growing importance for finer distinctions in flow velocity. When excluding the attack angle or using only pressure data, accuracy dropped to near-random levels, underscoring the attack angle's critical role. Furthermore, as the task complexity grew, the importance of specific pressure sensors became clearer. For example, excluding P_3 caused a sharp drop in accuracy, while excluding $P_{2,4}$ led to a smaller decline , highlighting P_3's crucial role in classification.

V. CONCLUSION

This paper presents an efficient data-driven framework that enables a robotic fish with an ALLS to classify ambient flow conditions while swimming freely. Instead of measuring exact flow velocities, the focus is on classifying flow into discrete categories, similar to how real fish prioritize relative flow magnitudes for adaptive swimming. This approach simplifies computation and broadens its applicability across different flow regimes and fish sizes. The novelty of our method lies in the integration of pressure data and motion parameters into an LSTM-based deep learning framework. Unlike other works that emphasize network or sensor optimization, our results show that selecting movement-related features significantly improves classification accuracy. Requiring only five pressure sensors and minimal data collection, this method achieves high accuracy, offering a flexible solution adaptable to various robotic fish sizes and dynamic environments.

Authorized licensed use limited to: ShanghaiTech University. Downloaded on March 10,2026 at 06:36:40 UTC from IEEE Xplore. Restrictions apply.

REFERENCES

[1] X. Zheng, W. Wang, M. Xiong, and G. Xie, "Online state estimation of a fin-actuated underwater robot using artificial lateral line system," *IEEE Transactions on Robotics*, vol. 36, no. 2, pp. 472–487, 2020.

[2] W. Tang, Y. Wang, Z. Yu, Z. Li, and J. Qu, "Bionic robotic fish mechanical structure optimization design and performance analysis based on fluent," in *2023 IEEE 19th International Conference on Automation Science and Engineering (CASE)*. IEEE, 2023, pp. 1–6.

[3] Y. Zhang, M. Ding, S. Zhu, Y. Liang, Y. Bai, K. Xie, M. Wan, J. Gu, and T. Li, "Conceptual design and simulation of a bcf swimming soft robotic fish for deep-sea," in *2022 IEEE International Conference on Robotics and Biomimetics (ROBIO)*. IEEE, 2022, pp. 111–115.

[4] T. Zhang, Y. Li, S. Li, Q. Ye, C. Wang, and G. Xie, "Decentralized circle formation control for fish-like robots in the real-world via reinforcement learning," in *2021 IEEE International Conference on Robotics and Automation (ICRA)*. IEEE, 2021, pp. 8814–8820.

[5] T. Hirayama, T. Kishimoto, and H. Takahashi, "Pitot tube type compact waterproof airflow sensor for seabird biologging," in *2023 IEEE SENSORS*. IEEE, 2023, pp. 1–4.

[6] Z. Yang, Z. Gong, Y. Jiang, Y. Cai, Z. Ma, X. Na, Z. Dong, and D. Zhang, "Maximized hydrodynamic stimulation strategy for placement of differential pressure and velocity sensors in artificial lateral line systems," *IEEE Robotics and Automation Letters*, vol. 7, no. 2, pp. 2170–2177, 2022.

[7] E. Marchetti, T. Culverhouse, T. Comerford, and A. Nimmo-Smith, "Validation of high-resolution adcp measurements of tke dissipation influenced by waves," in *2024 IEEE/OES Thirteenth Current, Waves and Turbulence Measurement (CWTM)*. IEEE, 2024, pp. 1–12.

[8] R. Venturelli, O. Akanyeti, F. Visentin, J. Ježov, L. D. Chambers, G. Toming, J. Brown, M. Kruusmaa, W. M. Megill, and P. Fiorini, "Hydrodynamic pressure sensing with an artificial lateral line in steady and unsteady flows," *Bioinspiration & biomimetics*, vol. 7, no. 3, p. 036004, 2012.

[9] Y. Jiang, Z. Ma, J. Fu, and D. Zhang, "Development of a flexible artificial lateral line canal system for hydrodynamic pressure detection," *Sensors*, vol. 17, no. 6, p. 1220, 2017.

[10] M. Asadnia, A. G. P. Kottapalli, K. D. Karavitaki, M. E. Warkiani, J. Miao, D. P. Corey, and M. Triantafyllou, "From biological cilia to artificial flow sensors: Biomimetic soft polymer nanosensors with high sensing performance," *Scientific reports*, vol. 6, no. 1, pp. 1–13, 2016.

[11] Y. Yang, J. Chen, J. Engel, S. Pandya, N. Chen, C. Tucker, S. Coombs, D. L. Jones, and C. Liu, "Distant touch hydrodynamic imaging with an artificial lateral line," *Proceedings of the National Academy of Sciences*, vol. 103, no. 50, pp. 18 891–18 895, 2006.

[12] J. Stocking, W. Eberhardt, Y. Shakhsheer, B. Calhoun, J. Paulus, and M. Appleby, "A capacitance-based whisker-like artificial sensor for fluid motion sensing," in *SENSORS, 2010 IEEE*. IEEE, 2010, pp. 2224–2229.

[13] Z. Zhang, C. Zhou, L. Cheng, X. Wang, and M. Tan, "Real-time velocity vector resolving of artificial lateral line array with fishlike motion noise suppression," *IEEE Transactions on Robotics*, 2023.

[14] S. Verma, C. Papadimitriou, N. Lüthen, G. Arampatzis, and P. Koumoutsakos, "Optimal sensor placement for artificial swimmers," *Journal of Fluid Mechanics*, vol. 884, p. A24, 2020.

[15] G. Liu, M. Wang, A. Wang, S. Wang, T. Yang, R. Malekian, and Z. Li, "Research on flow field perception based on artificial lateral line sensor system," *Sensors*, vol. 18, no. 3, p. 838, 2018.

[16] W. Wang, Y. Li, X. Zhang, C. Wang, S. Chen, and G. Xie, "Speed evaluation of a freely swimming robotic fish with an artificial lateral line," in *2016 IEEE International Conference on Robotics and Automation (ICRA)*. IEEE, 2016, pp. 4737–4742.

[17] C. Wang, W. Wang, and G. Xie, "Speed estimation for robotic fish using onboard artificial lateral line and inertial measurement unit," in *2015 IEEE International Conference on Robotics and Biomimetics (ROBIO)*. IEEE, 2015, pp. 285–290.

[18] G. Li, G. Liu, B. Jin, W. Wang, and X. Fang, "A new artificial lateral line attitude perception method based on mixed activation function-multilayer perceptron (maf-mlp)," *Ocean Engineering*, vol. 288, p. 116100, 2023.

[19] S. Coombs, H. Bleckmann, R. R. Fay, A. N. Popper, *et al.*, *The lateral line system*. Springer, 2014.

[20] T. Salumäe and M. Kruusmaa, "Flow-relative control of an underwater robot," *Proceedings of the Royal Society A: Mathematical, Physical and Engineering Sciences*, vol. 469, no. 2153, p. 20120671, 2013.

[21] J. F. Fuentes-Pérez, J. A. Tuhtan, R. Carbonell-Baeza, M. Musall, G. Toming, N. Muhammad, and M. Kruusmaa, "Current velocity estimation using a lateral line probe," *Ecological Engineering*, vol. 85, pp. 296–300, 2015.

[22] G. Liu, H. Hao, T. Yang, S. Liu, M. Wang, A. Incecik, and Z. Li, "Flow field perception of a moving carrier based on an artificial lateral line system," *Sensors*, vol. 20, no. 5, p. 1512, 2020.

[23] R. Liu, Y. Ding, and G. Xie, "Real-time position and pose prediction for a self-propelled undulatory swimmer in 3d space with artificial lateral line system," *Bioinspiration biomimetics*, vol. 19, 05 2024.

[24] Y. Hu, S. Zhang, J. Liang, and T. Wang, "Development and cpg-based control of a biomimetic robotic fish with advanced underwater mobility," in *2014 IEEE International Conference on Robotics and Automation (ICRA)*. IEEE, 2014, pp. 813–818.

[25] D. M. Powers, "Evaluation: from precision, recall and f-measure to roc, informedness, markedness and correlation," *arXiv preprint arXiv:2010.16061*, 2020.

Authorized licensed use limited to: ShanghaiTech University. Downloaded on March 10,2026 at 06:36:40 UTC from IEEE Xplore. Restrictions apply.